

Identifying liver cancer cells using cascaded convolutional neural network and gray level co-occurrence matrix techniques

Bellary Chiterki Anil¹, Arun Kumar Gowdru², Dayananda Prithviraja³,
Niranjan Chanabasappa Kundur⁴, Balakrishnan Ramadoss⁵

¹Department of Computer Science and Engineering (AI & ML), JSS Academy of Technical Education, Bengaluru, India

²Department of Electronics and Communication Engineering, JSS Academy of Technical Education, Noida, India

³Department of Information Technology, Manipal Institute of Technology, Manipal Academy of Higher Education, Manipal, India

⁴Department of Computer Science and Engineering, JSS Academy of Technical Education, Bengaluru, India

⁵Department of Computer Applications, National Institute of Technology, Tiruchirapalli, India

Article Info

Article history:

Received Jan 30, 2024

Revised Feb 20, 2024

Accepted Feb 28, 2024

Keywords:

Computed tomography
Hepatocellular carcinoma
Metastatic carcinoma
Convolutional neural network
Region of interest
Machine learning

ABSTRACT

Liver cancer has a high mortality rate, especially in South Asia, East Asia, and Sub-Saharan Africa. Efforts to reduce these rates focus on detecting liver cancer at all stages. Early detection allows more treatment options, though symptoms may not always be apparent. The staging process evaluates tumor size, location, lymph node involvement, and spread to other organs. Our research used the CLD staging system, assessing tumor size (C), lymph nodes (L), and distant invasion (D). We applied a deep learning approach with a cascaded convolutional neural network (CNN) and gray level co-occurrence matrix (GLCM)-based texture features to distinguish benign from malignant tumors. The method validated with the cancer imaging archive (TCIA) dataset, demonstrating superior accuracy compared to existing techniques.

This is an open access article under the [CC BY-SA](#) license.



Corresponding Author:

Arun Kumar Gowdru

Department of Electronics and Communication Engineering, JSS Academy of Technical Education

Noida, India

Email: arunkumargowdru.1981@gmail.com

1. INTRODUCTION

Liver tissue cancer, a malignancy characterized by the proliferation of cancerous cells within the liver, presents a significant challenge. The aim of this analysis is to accurately identify cancerous regions and estimate size of malignant tissue from “computed tomography (CT)” scan slices. These slices cover the liver and adjacent internal organs, spanning from top to bottom. Through segmentation of each slice, volumetric measurements of the entire liver can be obtained, facilitating the assessment of affected tissue extent at different stages of cancer progression, as detailed in Table 1 (see in Appendix). Liver cancer constitutes a health concern globally, with a high risk of recurrent occurrences. In 2020 alone, there were approximately 9.5 lakh newly diagnosed cases of liver cancer annually, ranking it as the fourth leading cause of cancer-related deaths worldwide across all income brackets. According to the WHO global cancer data, projections for 2019 indicated around 8.7 million new cases of cancer diagnosed globally, resulting in around 9.8 million deaths.", with liver cancer contributing to approximately 8.2%, or roughly 782,000 deaths.

2. RELATED WORK

The researchers explored various convolutional network architectures for subdivision and tumor recognition purposes. The primary focus of the study was to assess the recital of U-Net and SegNet. Results

exhibited that the model achieved a promising dice for each case score of 69.79, indicating its effectiveness in the breakdown process [1]. Additionally, the researchers found that SegNet outperformed U-Net in liver segmentation, achieving a dice score of 95.53. Furthermore, the research demonstrated that incorporating an additional classifier for tumor recognition significantly improved the results, particularly in the separation of irregular tissues. This finding adds further validation to the efficacy of utilizing U-Net for lesion separation tasks involving tumor-ridden livers [2]. The authors emphasized importance of automatic liver lesion segmentation for achieving effective treatment outcomes and assisting medical experts. They proposed a cascaded system utilizing both 3D and 2D “convolutional neural networks (CNN)” to segment hepatic lesions. To appraise the segmentation results, a two-fold cross-validation was conducted on the liver tumor segmentation benchmark (LiTS) dataset, aiming to identify any possible issues associated to under-segmentation or over-segmentation [3].

This work presents a innovative technique for identification of liver cancer lumps and analyzing their severity automatically. The usage of hybrid traits, rendering to the researchers, could help identify malignant spots. The methodology encompasses some steps, opening with pre-processing analysis using median filtering. This is followed by binary segmentation based on dynamic thresholding, and identification of the “region of interest” (ROI) through the application of morphological functions. The simulation outcomes demonstrate that the proposed model enhances the precision of detection with minimal computational overhead. The achieved accuracy is reported as 92.67%, and the average detection time is 1.13 seconds. These results highlight the efficiency of the projected model in accurately detecting cancer tumors [4]. In this research paper, the researchers propose an optimization technique designed for the automatic recognition of tumor in abdominal liver images. These techniques significantly improve the efficacy of tumor segmentation, contributing to more accurate detection. Notably, the water shed algorithm is specifically employed in this analysis, yielding an impressive average accuracy of 0.97. Overall, this paper presents an optimization technique that offers automated cancer detection in liver metaphors of abdomen [5]

Machine learning has emerged as a prevailing tool in biomedical imaging, particularly in the medicinal tomography field. By employing machine learning methods for disease detection and cancer cell identification, researchers have produced excellent results. In this study, the focus is on femur segmentation. The researchers employed femur segmentation, a process that involves delineation and identification of the femur bone in medical images. The projected technique yielded hopeful results, a dice value of 0.95 and with a quick processing period of 0.93 seconds [6].

Experimental work offered here goals to adapt a deep learning prototype used for semantic segmentation of road scenes to the segmentation of CT liver scan tumors in digital imaging and communications in medicine (DICOM) format. With SegNet, image-level classification is accomplished by pixel-level features using the trained VGG-16 image classification network as encoder and decoding architecture as decoder. As opposed to conventional auto-encoders, SegNet saves only the max-pooling indexes of feature maps instead of the entire maps. Most tumor parts can be correctly perceived by the proposed method with an accuracy rate of over 86%. Although some false positives could be lowered by applying false positive filters and training the model with more data, based on results, it appears that some could be reduced by applying false positive filters [7]

The network architecture and training cases were optimized to generate a custom CNN, and the final network consisted of three convolutional layers with remedied linear units, two maximum pooling and 2 fully linked layers. 494 hepatic lesions with typical imaging features were used in total, divided into training (n=434) and testing (n=60). Cross-validation with Monte Carlo was used. Following the completion of model engineering, the classification accurateness of the final CNN was compared with two board-certified radiologists on an identical unseen test set. The DLS achieved 92% accuracy, 92% sensitivity (Sn), and 98% specificity (Sp). In a single run of random unseen cases, test set performance averaged 90% Sn and 98% Sp. For radiologists, the average Sn/Sp on these same cases was 82.5%/96.5%. The results showed a 90% Sn for classifying hepatocellular carcinoma (HCC) compared to 60%/70% for radiologists. False and true positive rates for HCC classification were 1.6% and 93.6%, respectively with a receiver working characteristic extent under the curvature of 0.992 [8].

Using 494 lesions on multi-phasic magnetic resonance imaging (MRI), as discussed, a CNN was created and trained to classify six hepatic tumour entities. Up to four important imaging features per lesion were used to label a portion of each lesion class. Additionally, each detected characteristic received a relevance score indicating its relative importance in the projected lesion classification. In identifying the correct radiological features present in each test lesion, the interpretable deep learning system achieved 76.5% positive prognostic value and 82.9% sensitivity. The model misclassified 12% of lesions. Misclassified lesions had more incorrect features than correctly identified lesions (60.4% vs. 85.6%). The feature maps matched original image voxels that contributed to each imaging feature. Most significant imaging standards for each class were reflected in the feature relevance scores [9].

With increasing analysis applying CNNs in carcinoma pictures there's a requirement to value rigorously their accuracy and outline future research directions. whereas current studies have lined major liver cancers, the quantity of studies conducted up to now is little and limited, and a lot of research is required to answer questions about the accurateness and compassion of CNN algorithms. However, many deficiencies in current studies were observed. This be particularly vital in sight of the growing demand of CNNs in liver medical specialty. Azer [10] propose a procedure for tumor breakdown of liver that involves several stages, from preliminary to ultimate stage. The process begins with preprocessing steps, including grayscale translation and median filtering, to eliminate clutter from the input images. Then, CNN is employed to sector the liver section from CT images. Following the segmentation, the segmented CT volumes undergo feature mining using procedures such as gray level co-occurrence matrix (GLCM) shape features, and “local binary patterns (LBP)”. These features capture important appearances of the lump regions.

In this research analysis the research work introduces a novel approach for generating distinct categories of polyp intrants, providing valuable evidence of liver sections in CT images. This method incorporates a super pixel breakdown technique, enabling the mining of crucial and meaningful information pertaining to the liver region. By reducing redundant information within the liver regions, the effectiveness of the obtained information is enhanced, resulting in reduced computational complexity. In addition, the abstraction of liver tumor cells was carried out with remarkable efficiency through the utilization of the GLCM, shape features, and LBP. These advanced techniques, combined with application of active contouring, facilitated the precise refinement of the extracted tumor cells.

3. METHOD

Figure 1 demonstrates the comprehensive flowchart representing segmentation of anticipated liver tumour process. The process instigates with pre-processing of images, involving crucial steps such as grayscale translation and median filtering. Subsequently, part of the liver is segmented using a CNN, ensuring accurate delineation.

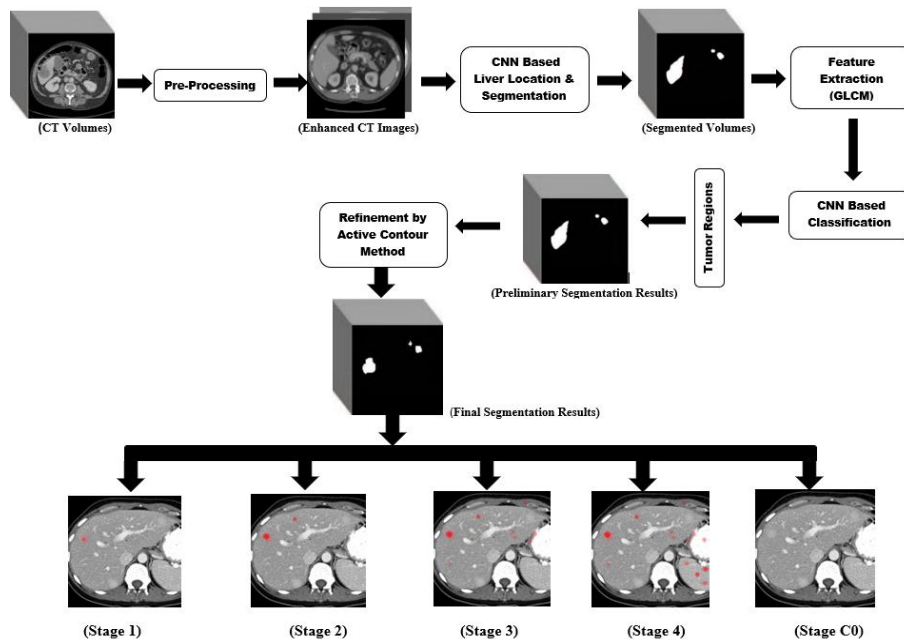


Figure 1. Flow chart: Feasible technique

Step 1: CT scans undergo preprocessing, which involves procedures such as grayscale translation and median filtering.

Recent automated deep learning-based techniques, designed without incorporating pre-processing analysis or similar approaches, may not exhibit the desired level of reliability when applied to larger databases or extensive timeframes. It is well-established that CT volumes contain various types of noise, such as impulse, and gaussian quantization noise. The initial step focuses on fine-tuning low-contrast CT images through an intensity value tuning function, which aims to mitigate noise-related challenges and improve complete recital of deep learning model.

$$X = \text{imadjust}(Y) \quad (1)$$

$$X = \text{imadjust}(Y, [L_in, H_in]) \quad (2)$$

$$X = \text{imadjust}(Y, [L_in, H_in], [L_out, H_out]) \quad (3)$$

In (1) enhances the dissimilarity of output image X by mapping intensity values from grayscale image Y to new values within the range of b . By evasion, the imadjust function saturates the top 1% and bottom 1% of all pixel values. In (2), L_in and H_in denote the lower and higher input values, respectively, both mapped to 0 and 1. In (3) extends this idea by mapping values between L_in and H_in to the range between L_out and H_out , aiming to minimize noise and artifacts effectively.

Step 2: after eliminating noise in the previous step, we employ a CNN to segment the CT volumes and extract the liver region [11].

Our method employs CNN to implement time implied phase growth for liver recognition and segmentation, representing a notable advancement over prior techniques using CNN for this purpose. Figure 2 demonstrates the utilization of convolutional filters and neural network connections in our approach, crucial for precise and efficient liver analysis. "A CNN method tailored for 2D abdominal liver segmentation was proposed to ensure precision in segmenting liver from CT scan images. This approach integrates classifiers and creators to delineate "non-liver" and "liver" regions using two-way layers with softmax probabilities. The CNN architecture comprises five layers, amalgamating information from five input images, while subsequent layers employ fully connected neural networks or max-pooling techniques to refine features. Employing canonical residual networks (ResNet) as encoders, global convolutional networks (GCNs) for decoding, and PatchGANs as classifiers, the system achieves high-resolution segmentation. DICOM images, acquired noncontinuously in an axial manner, are converted to neuroimaging informatics technology initiative (NIFTI) format to reconstruct 3D volumes. Additionally, each axial slice within a 3D CT volume is resized to 256 by 256 for testing and training purposes. The subsequent section elaborates on identifying malignant tumors through tumor candidate generation in segmented regions, with Figure 3 displaying obtained segmentation outcomes.

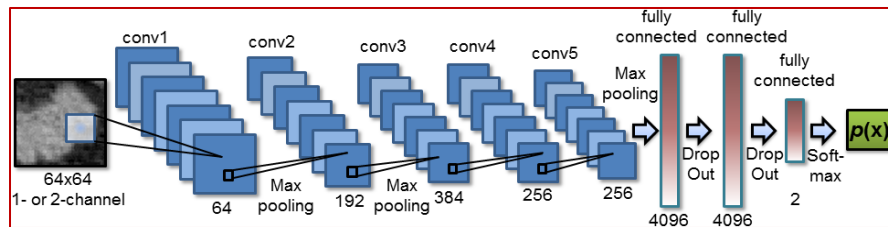


Figure 2. Convolution neural network architecture

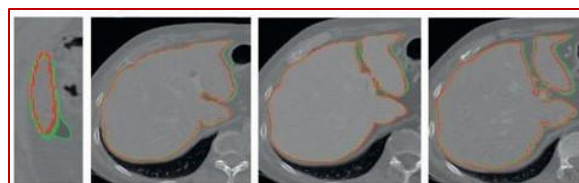


Figure 3. Segmentation results (green outline indicates physically recognized boundary and red outline signifies automatically recognized boundary)

Step 3: to efficiently extract the ROI from the segmented liver part, we utilize the GLCM-CNN approach.

This method focuses on capturing the distribution of grey levels, which represents the illumination values of pixels within an image. The GLCM technique is employed to gather information about image texture structures. Specifically, the GLCM considers spatial associations between two pixels at a specific orientation angle and distance. The GLCM matrix function is obtained by calculating the occurrence of pixel pairs with a certain distance (D) and orientation angle (θ), such as 0, 45, 90, and 120 degrees. This work utilizes several properties of the GLCM, namely homogeneity, energy, and contrast [12]. Homogeneity, also known as the inverse difference moment, is the reciprocal of contrast and measures the distribution of

elements along the GLCM diagonal. In (4) can be used to calculate homogeneity. Energy, also referred to as uniformity, quantifies the concentration of gray levels in the GLCM. It represents the number of squared elements in the GLCM and can be computed using (5) and (6) can be used to calculate contrast. In (4)-(6), the vertical and horizontal coordinates in the GLCM matrix are represented by 'a' and 'b', respectively, and the matrix value at coordinate (a, b) is denoted by M (a, b).

$$H = \frac{\sum_{a,b=1}^X M_{a,b}}{1+(a+b)^2} \tag{4}$$

$$E = \sum_{a,b=1}^X M_{a,b^2} \tag{5}$$

$$C = \sum_{a,b=1}^X M_{a,b} (a - b)^2 \tag{6}$$

By incorporating GLCM texture features into the input layer, an improved technique of the CNN is presented, as depicted in Figure 4, which showcases the architecture of GLCM-CNN. In the first layer, an image of size 228×344 pixels are obtained from features extracted using the GLCM method. It is calculated based on the major axis length (a) and minor axis length (b) and is represented by (7). Perimeter is another feature that determines the boundary span of the ROI and generates an array where pixels with 255 values indicate the “border and pixels with 0 values indicate the interior. In (8) represents the perimeter calculation, with A and B representing the edges of the ROI. Additionally, trajectory represents the arrangement of pixels (ath and bth) by generating corresponding curvatures. Lastly, the important feature of area is calculated using (9), where a and b represent the number of pixels within the shape. An ROI vector is constructed, consisting of a ROI at position A and a ROI at position B [13], [14]. These GLCM texture features contribute to the overall classification performance of the GLCM-CNN model.

$$E = \frac{a}{b} \tag{7}$$

$$P = (P_{a,b}, A \text{ edge } [P] = a, B \text{ edge } [P] = b) \tag{8}$$

$$A = (A_{a,b}, A \text{ ROI } [Area] = a, B \text{ ROI } [Area] = b) \tag{9}$$

The modified technique depicted in Figure 4 is referred to as GLCM-CNN, with the architecture consisting of sub-sampling layers and three types of layers: convolutional layers followed by an output layer. The purpose of using the GLCM is to extract features that characterize a set of structures, this helps decrease the misclassification of cancerous tumors in images. In (10) outlines the sub-sampling function, wherein the input patch window function denotes the neighborhood X(n, n), and calculates the average value of this neighborhood. The output layer is directly linked to the last convolutional layer and comprises four to five neurons, each representing various stages of cancer. This layer produces the ultimate output utilizing the acquired features, thereby facilitating the classification process.

$$A_j = \text{avg}_{n*n} (A_j^{n*n} * X(n, n)) \tag{10}$$

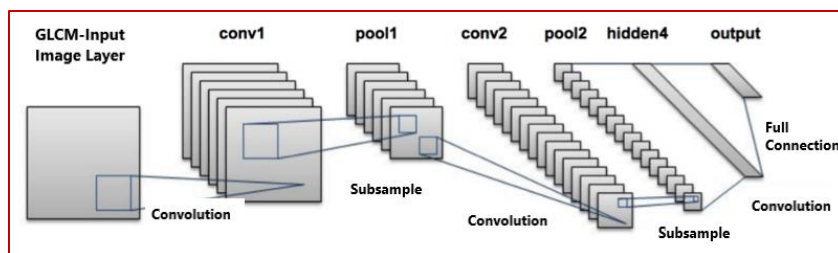


Figure 4. Architecture of GLCM-CNN

During CNN training, the objective is to minimize the average squared error obtained from the training data. In (11) defines the average squared error, where X represents the total number of training data samples, d_j(n) denotes the target of the actual class, B stands for the number of batches, y_j(n) signifies the output of the jth layer, and E_average indicates the normalized value of the squared error.

$$E_{\text{average}} = \frac{1}{X} \sum_{a=1}^B (d_j(n) - y_j(n))^2 \tag{11}$$

Step 4: Active contour method is utilized for refining the identification of liver tumors [15]

Anil and Dayananda [11] presented a comprehensive convex active contour model (ACM) for reflex image segmentation to refine the boundaries obtained in step 3 of our methodology. This technique involves three main steps: contour Initialization, regional term formulation, and boundary term formulation. The ACM is utilized to enhance and fine-tune the tumor boundaries. It aims to recover lost borders or eliminate unwanted borders from the image. The function h_r is a region function that evaluates the exterior and interior regions based on specific constraints. The function u operates on the image domain and assigns a value between 0 and 1 to each pixel position x in the image. For a detailed explanation of this step, please refer to [11].

$$\min_{0 \leq u \leq 1} \left(\int_{\Omega} g_b |\nabla u| dx + \lambda \int_{\Omega} h_r u dx \right) \tag{12}$$

4. RESULTS AND DISCUSSION

In this section, we conducted a comprehensive comparison and evaluation of various segmentation techniques vis-à-vis our proposed method. Through meticulous analysis and comparison with other methodologies [16]–[19], we have established that our segmentation approach outperforms these methods, exhibiting a notable improvement in dice precision ranging from 6% to 10%. In (13) delineates the accuracy calculation. It's important to note that the specific equations and intricacies regarding accuracy computation may vary depending on the methodology elucidated in the original papers [16]–[19]. For a more thorough understanding, we recommend referring to the original research papers for a detailed explanation of the accuracy calculation methodology.

$$A = \frac{\text{No.of correct identification}}{\text{total number of test data}} \times 100 \tag{13}$$

Table 2 also features the maximum and minimum values for each category of tumors. It's crucial to emphasize that without access to the actual table and specific data, we unable to provide exact scores and comparisons for each metric. Figures 5 and 6 provides a quantitative evaluation of the proposed segmentation technique, comparing it to CNN and GLCM-CNN methods. Analysis from the table reveals that the GLCM-CNN method achieves higher accuracy. Table 3 shows the classification precision of two models: CNN and GLCM-CNN. Table 4 further presents an assessment of the proposed segmentation procedure, analyzing segmentation results for small, medium, and large tumors. Metrics such as relative volume differences (RVD), dice per case, volume overlap error (VOE), average symmetric difference (ASD), and maximum symmetric difference (MSD) are utilized to quantify the scores [20]–[22]. Nevertheless, this table facilitates a thorough assessment of the segmentation results, offering valuable insights into the performance of the proposed segmentation technique [23]–[25] across various tumor sizes. For detailed information and precise values.

Table 2. Segmentation results comparison with other approaches

Method/Author	Dice per case	ASD (mm)	RVD	VOE	MSD (mm)
Chris <i>et al.</i> [16]	0.56	-	-	-	-
Yuan <i>et al.</i> [17]	0.56	1.151	0.228	0.378	6.269
Chlebus <i>et al.</i> [18]	0.65	11.11	0.380	0.625	16.71
Chen <i>et al.</i> [6]	0.67	6.36	0.41	0.564	11.69
Proposed method [CNN+GLCM]	0.86	4.753	0.234	0.312	10.21

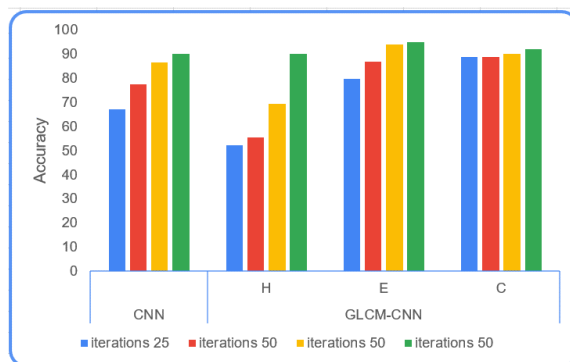


Figure 5. Graphical representation of classification precision of CNN and GLCM-CNN

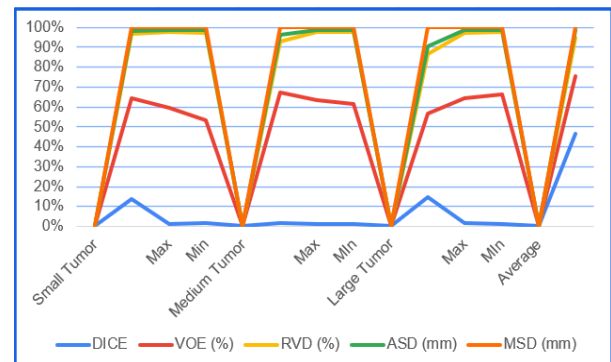


Figure 6. Graphical illustration of scores (Table 4)

Table 3. Classification precision of CNN and GLCM-CNN

Iterations	CNN	GLCM-CNN		
		H	E	C
25	66.78	52.16	79.65	88.69
50	77.25	55.24	86.63	88.62
100	86.34	69.23	93.65	89.72
200	89.89	89.91	94.65	91.76

Table 4. Evaluation of the proposed tumor segmentation technique quantitatively

	DICE	VOE (%)	RVD (%)	ASD (mm)	MSD (mm)
Small tumor	0.87 ± 2.25	36.91 ± 8.26	24.69 ± 5.36	0.76 ± 0.21	0.98 ± 0.30
Max	0.87	44.65	29.31	0.91	0.92
Min	0.71	24.12	20.62	0.54	0.69
Medium tumor	0.81 ± 0.25	37.62 ± 9.62	22.54 ± 3.72	0.73 ± 0.51	1.14 ± 0.52
Max	0.91	46.03	25.56	0.85	0.86
Min	0.73	32.45	19.62	0.56	0.68
Large tumor	0.91 ± 1.25	38.95 ± 3.62	19.23 ± 2.56	0.78 ± 0.32	1.12 ± 0.84
Max	0.94	41.53	21.79	0.92	0.85
Min	0.75	35.31	17.23	0.52	0.67
Average	0.87 ± 7.06	28.05 ± 4.32	23.25 ± 2.95	0.77 ± 0.56	1.11 ± 0.21

5. CONCLUSION

Liver cancer, the deadliest form globally, demands precise analysis and swift tumor identification across all stages to improve survival rates. A new method, using CT scan images, is being developed to detect liver cancer stages efficiently. Initial steps involve image preprocessing, converting to grayscale and applying median filtering. A novel segmentation technique, including CNN, accurately segments cancerous polyps. Key properties like eccentricity, perimeter, and area are extracted using the GLCM method from the segmented ROI. The ACM refines tumor localization. This combined approach has shown promising results, achieving a dice similarity coefficient of $81.8 \pm 14.5\%$ during training and $80.6 \pm 12.9\%$ during testing on CT images from 132 patients.

APPENDIX

Table 1. Different stages of cancer

Stage	Stage grouping	Stage description
1	C0	C0 indicates No evidence of a primary tumor.
1A	C1a	C1a indicates not grown to blood vessels and it is only tumor size varies from 1-2 cm.
	L0	L0 indicates has not spread to nearby lymph nodes.
1B	D0	D0 indicates has not spread to distant sites.
	C1b	C1b indicates not grown to blood vessels and it is only tumor size varies from 2-4 cm.
2	L0	L0 indicates has not spread to nearby lymph nodes.
	D0	D0 indicates has not spread to distant sites.
	C2	C2 indicates may be growth of single tumor, size is great than 2 cm and parallely has grown into blood vessels or may be grown of more than one tumor but not larger than 6cm.
3A	L0	L0 indicates has not spread to nearby lymph nodes.
	D0	D0 indicates has not spread to distant sites.
	C3	C3 indicates growth of more than one tumor, size is great than 6 cm
3B	L0	L0 indicates has not spread to nearby lymph nodes.
	D0	D0 indicates has not spread to distant sites.
4A	Any C	L1 indicates growth of single tumour or multiple tumors of any size has blowout to neighboring lymph nodes.
	L1	D0 indicates has not blowout to detached sites.
4B	Any C	D1 indicates It has spread to detached organs such as the bones or lungs.
	Any L	
	D1	




REFERENCES

- [1] E. Smith, "World cancer day 2017: liver cancer, a global challenge thanks to viruses and alcohol," *Cancer Research UK*, 2017, Accessed: Jun. 10, 2018. [Online]. Available: <https://news.cancerresearchuk.org/2017/02/13/world-cancer-day-2017-liver-cancer-a-global-challenge-thanks-to-viruses-and-alcohol/>
- [2] N. Nanda, P. Kakkar, and S. Nagpal, "Computer-aided segmentation of liver lesions in CT scans using cascaded convolutional




- neural networks and genetically optimised classifier,” *Arabian Journal for Science and Engineering*, vol. 44, no. 4, pp. 4049–4062, 2019, doi: 10.1007/s13369-019-03735-8.
- [3] R. Dey and Y. Hong, “Hybrid cascaded neural network for liver lesion segmentation,” in *2020 IEEE 17th International Symposium on Biomedical Imaging (ISBI)*, 2020, pp. 1173–1177, doi: 10.1109/ISBI45749.2020.9098656.
 - [4] S. I. Turab and V. K. Kadam, “Liver cancer detection and grading using efficient computer vision techniques,” *Annals of the Romanian Society for Cell Biology*, vol. 25, no. 2, pp. 1740–1755, 2021.
 - [5] A. Krishan and D. Mittal, “Ensembled liver cancer detection and classification using CT images,” *Proceedings of the Institution of Mechanical Engineers, Part H: Journal of Engineering in Medicine*, vol. 235, no. 2, pp. 232–244, 2021, doi: 10.1177/0954411920971888.
 - [6] F. Chen, J. Liu, Z. Zhao, M. Zhu, and H. Liao, “Three-dimensional feature-enhanced network for automatic femur segmentation,” *IEEE Journal of Biomedical and Health Informatics*, vol. 23, no. 1, pp. 243–252, 2019, doi: 10.1109/JBHI.2017.2785389.
 - [7] S. Almotairi, G. Kareem, M. Aouf, B. Almutairi, and M. A. M. Salem, “Liver tumor segmentation in CT scans using modified segnet,” *Sensors*, vol. 20, no. 5, 2020, doi: 10.3390/s20051516.
 - [8] C. A. Hamm *et al.*, “Deep learning for liver tumor diagnosis part I: development of a convolutional neural network classifier for multi-phasic MRI,” *European Radiology*, vol. 29, no. 7, pp. 3338–3347, 2019.
 - [9] C. J. Wang *et al.*, “Deep learning for liver tumor diagnosis part II: convolutional neural network interpretation using radiologic imaging features,” *European Radiology*, vol. 29, no. 7, pp. 3348–3357, 2019, doi: 10.1007/s00330-019-06214-8.
 - [10] S. A. Azer, “Deep learning with convolutional neural networks for identification of liver masses and hepatocellular carcinoma: A systematic review,” *World Journal of Gastrointestinal Oncology*, vol. 11, no. 12, pp. 1218–1230, 2019, doi: 10.4251/wjgo.v11.i12.1218.
 - [11] B. C. Anil and P. Dayananda, “Automatic liver tumor segmentation based on multi-level deep convolutional networks and fractal residual network,” *IETE Journal of Research*, vol. 69, no. 4, pp. 1925–1933, 2023, doi: 10.1080/03772063.2021.1878066.
 - [12] U. Hameed, M. U. Rehman, A. Rehman, R. Damaševičius, A. Sattar, and T. Saba, “A deep learning approach for liver cancer detection in CT scans,” *Computer Methods in Biomechanics and Biomedical Engineering: Imaging & Visualization*, vol. 11, no. 7, 2024, doi: 10.1080/21681163.2023.2280558.
 - [13] X. Jia and M. Q. H. Meng, “A deep convolutional neural network for bleeding detection in wireless capsule endoscopy images,” in *2016 38th Annual International Conference of the IEEE Engineering in Medicine and Biology Society (EMBC)*, 2016, pp. 639–642, doi: 10.1109/EMBC.2016.7590783.
 - [14] K. Suzuki, J. Shiraishi, H. Abe, H. MacMahon, K. Doi, “False-positive reduction in computer-aided diagnostic scheme for detecting nodules in chest radiographs by means of massive training artificial neural network,” *Academic Radiology*, vol. 12, no. 2, pp. 191–201, 2005, doi: 10.1016/j.acra.2004.11.017.
 - [15] M. Kass, A. Witkin, and D. Terzopoulos, “Snakes: active contour models,” *International Journal of Computer Vision*, vol. 1, no. 4, pp. 321–331, 1988, doi: 10.1007/BF00133570.
 - [16] P. F. Christ *et al.*, “Automatic liver and tumor segmentation of CT and MRI volumes using cascaded fully convolutional neural networks,” *Arxiv-Computer Science*, vol. 1, pp. 1–20, 2017.
 - [17] Y. Yuan, “Hierarchical convolutional-deconvolutional neural networks for automatic liver and tumor segmentation,” *Arxiv-Computer Science*, pp. 1–4, 2017.
 - [18] G. Chlebus, H. Meine, J. H. Moltz, and A. Schenk, “Neural network based automatic liver tumor segmentation with random forest-based candidate filtering,” *Arxiv-Computer Science*, vol. 1, no. 1–4, 2017.
 - [19] X. Han, “Automatic liver lesion segmentation using a deep convolutional neural network method,” *Arxiv-Computer Science*, vol. 1, pp. 1–4, 2017.
 - [20] K. He, X. Zhang, S. Ren, and J. Sun, “Deep residual learning for image recognition,” in *2016 IEEE Conference on Computer Vision and Pattern Recognition (CVPR)*, 2016, pp. 770–778, doi: 10.1109/CVPR.2016.90.
 - [21] C. Peng, X. Zhang, G. Yu, G. Luo, and J. Sun, “Large kernel matters—improve semantic segmentation by global convolutional network,” in *IEEE Conference on Computer Vision and Pattern Recognition (CVPR)*, 2017, pp. 4353–4361.
 - [22] P. Isola, J.-Y. Zhu, T. Zhou, and A. A. Efros, “Image-to-image translation with conditional adversarial networks,” in *IEEE Conference on Computer Vision and Pattern Recognition (CVPR)*, 2017, pp. 1125–1134.
 - [23] M. M. Santoni, D. I. Sensuse, A. M. Arymurthy, and M. I. Fanany, “Cattle race classification using gray level co-occurrence matrix convolutional neural networks,” *Procedia Computer Science*, vol. 59, pp. 493–502, 2015, doi: 10.1016/j.procs.2015.07.525.
 - [24] S. S. Roy, S. Roy, P. Mukherjee, and A. H. Roy, “An automated liver tumour segmentation and classification model by deep learning based approaches,” *Computer Methods in Biomechanics and Biomedical Engineering: Imaging & Visualization*, vol. 11, no. 3, pp. 638–650, 2023, doi: 10.1080/21681163.2022.2099300.
 - [25] M. Hussain, N. Saher, and S. Qadri, “Computer vision approach for liver tumor classification using CT dataset,” *Applied Artificial Intelligence*, vol. 36, no. 1, 2022, doi: 10.1080/08839514.2022.2055395.

BIOGRAPHIES OF AUTHORS






Bellary Chiterki Anil    is working as Associate Professor & Head, Department of Computer Science and Engineering (AI & ML), JSS Academy of Technical Education, Bengaluru. He has completed B.E. degree in CSE Engineering (VTU) from RYMEC, Bellary, Karnataka, M.Tech. in CSE from SBMJCE, Karnataka, and Ph.D. in CSE Engineering from VTU, Belagavi in 2021. He has a teaching experience of more than 10 years. His area of research works are data mining and image processing. He has published over 25 papers in international journals and conferences. He is a member of CSI, ISTE societies in India. He is a reviewer for International Journals and conferences. He can be contacted at email: anil.bc2@gmail.com.






Arun Kumar Gowdru    is working as Professor & HOD, Department of ECE, JSSATE, NOIDA, UP. He has completed Diploma in E&C Engineering from Bapuji Polytechnic, Davanagere, B.E. degree in ECE (VTU) from STJIT, Ranebennur, Karnataka, M.Tech. in Digital Communications & Networking from Govt. UBDCET, Davanagere, Karnataka, and Ph.D. in ECE from VTU, Belagavi in 2016. He has a teaching experience of more than 16 years. He can be contacted at email: arunkumargowdru.1981@gmail.com.






Dayananda Pruthviraja    is currently working as professor & HOD in the Department of IT at MITB. He Obtained PhD degree from VTU and MTech degree from RVCE. His focus area is image processing & information retrieval. He was with MSRIT, Bengaluru, India. He has published many papers in national and international journals in the field of image processing and retrieval. He can be contacted at email: dayananda.p@manipal.edu.



Niranjana C. Kundur    holds a Doctorate of Computer and Information Sciences from VTU University, India in 2023. He is currently an associate professor at Department of Computer Science in JSS ATEB, VTU University, India. His research includes computer vision, pattern recognition, machine learning, data mining, deep learning, and artificial intelligence. He has published over 30 papers in international journals and conferences. He is a member of IAENG and ISTE societies in India. He is a reviewer for international journals and conferences. He can be contacted at email: niranjankundur@jssateb.ac.in or niranjankt@gmail.com.



Balakrishnan Ramadoss    received the M.Tech. degree in CSE in 1995 from the IIT, Delhi and the Ph.D. degree in Applied Mathematics in 1983 from IIT, Bombay. Currently, he is working as a Professor (HAG) Computer Applications at NIT, Tiruchirappalli. He has 30+ years of teaching & research experience. Under his guidance, 13 have successfully completed Ph.D. programme. He has 80+ research publications in SCI/SCIE/Scopus and reputed international conferences. His research interests include security and privacy in big data and cloud, software testing, and information retrieval. He can be contacted at email: brama@nitt.edu.